3-D Numerical Modeling of the Thermo-Inductive Technique Using Shell Elements

Brahim Ramdane, Didier Trichet, Mohamed Belkadi, and Javad Fouladgar

Institut de Recherche en Electrotechnique et Electronique de Nantes Atlantique (IREENA), 37, Boulevard de l'université, BP 406-44600 Saint Nazaire Cedex, France

Thermo-inductive testing is a new technique used for health investigations on different components of automotive and aeronautic industries. In this technique, eddy current deviation around the default creates local heating which can be detected by an infrared camera. The purpose of this work is to develop a 3-D finite-element model as a support tool to study the reliability of the technique. To reduce the number of unknowns, shell elements are introduced to model defects or thin conductive regions. Inspected materials are classified into metallic and composites. Investigations on various parameters of the technique and crack dimensions are performed in order to optimize the method. Experimental and simulation results show that the method is well suited.

Index Terms—**Eddy current testing, finite-element methods, induction heating, infrared measurements, nondestructive testing.**

I. Introduction

CRACKS constitute one of the major problems threatening the security of systems subjected to mechanical, thermal or chemical constraints. In order to detect and characterize these defects in different materials and situations, researches try to combine the NDT techniques to obtain the best performances. In this context, we propose a new method called thermo-inductive technique, which combines the advantages of both eddy current and infrared thermography techniques [1].

This technique is recent and little researches are carried out on it in the literature. In addition, most of these works are based on simplified models which limit the study to simple types of defects and pieces [2]. Our objective is then to develop a 3-D numerical model as a support tool to analysz and optimize this new technique.

The ability of thermo-inductive method to detect the defects depends on electromagnetic and thermal properties of the material under investigation. In automotive and aeronautic industry, two principal groups of material are used: metallic pieces and carbon fiber reinforced polymer composite sheets. The first group has a linear or non linear magnetic permeability, a small electromagnetic skin depth and high thermal diffusivity. The second group has non isotropic physical properties, high skin depth and low thermal diffusivity.

The material investigated by this technique present a scale factor problem at two levels. The cracks but also the material itself which may be large and thin such as aluminium plates or composite sheets. Modeling such regions involves difficulties due to their small thickness compared to other dimensions. This is expressed by mesh problems such as high density or deformed elements leading to a prohibitive computing time or ill-conditioned matrix systems. In literature, many researches have been carried out to model thin regions. Among the various proposed methods, the shell elements, which derive from degeneration of Whitney prism elements, is well suited for our problem [3].

Manuscript received December 18, 2009; accepted February 13, 2010. Current version published July 21, 2010. Corresponding author: B. Ramdane (e-mail: brahim.ramdane@univ-nantes.fr).

Color versions of one or more of the figures in this paper are available online at http://ieeexplore.ieee.org.

Digital Object Identifier 10.1109/TMAG.2010.2044022

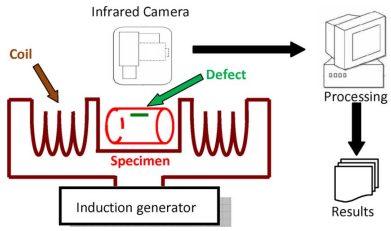

Fig. 1. Schematic of experimental system.

To consider all these constraints, we have developed a 3-D finite-element method based on Whitney's elements under a Matlab environment as a support tool to model the different phenomena involved in this technique. This model takes into account the anisotropy, the nonlinearity of materials, and the presence of thin regions which are modeled by the shell elements.

The new technique is applied to defects detection in materials used in automotive and aeronautic industries. Due to their anisotropic properties and scale factor, composite materials are modeled after a preliminary homogenization stage. The sensibility of the defect detection towards some parameters such as electromagnetic frequency, heating time, or defect dimensions has been investigated.

II. Problem Description

A typical measurement installation for the thermo-inductive method is shown in Fig. 1. In this technique, the electromagnetic and thermal fields penetrations have a great influence on the defect detection. These two parameters depend on the field and thermal frequencies as well as the material physical properties. This is why the optimal field and thermal frequencies depend on the material under investigation. The induction frequency may vary from 50 Hz to 2 MHz and the thermal frequency from 0.1 to 20 Hz.

III. Numerical Modeling

The study of the NDT by thermo-inductive technique involves both thermal and electromagnetic phenomena.

A. Electromagnetic Model

The electromagnetic problem defined by Maxwell's equations is solved with the 3-D finite-element method. The weak

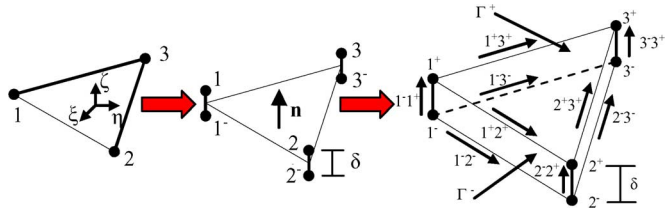

Fig. 2. Degeneration of regular prism elements to shell elements.

$\mathbf{T}-\Phi$ formulation in harmonic state is expressed by [4], [5]

$$\int_{\Omega_C}\left([\sigma]^{-1}\mathbf{Curl}\,\mathbf{w_{e_i}}\cdot\mathbf{Curl}\,\mathbf{T}+j\omega[\mu]\mathbf{w_{e_i}}\cdot(\mathbf{T}-\mathbf{grad}\,\Phi)\right)\cdot d\Omega$$
$$=\int_{\Omega_C}\left([\sigma]^{-1}\mathbf{Curl}\,\mathbf{w_{e_i}}\cdot\mathbf{Curl}\,\mathbf{T_0}+j\omega[\mu]\mathbf{w_{e_i}}\cdot\mathbf{T_0}\right)\cdot d\Omega \quad (1)$$
$$-\int_{\Omega_C}j\omega[\mu]\mathbf{grad}\,w_{n_i}\cdot\mathbf{T}\cdot d\Omega+\int_{\Omega}j\omega[\mu]\mathbf{grad}\,w_{n_i}\cdot\mathbf{grad}\,\Phi\cdot d\Omega$$
$$=\int_{\Omega}j\omega[\mu]\mathbf{grad}\,w_{n_i}\cdot\mathbf{T_0}\cdot d\Omega \quad (2)$$

where $[\mu]$ represents the tensor of magnetic permeabilities, and $[\sigma]$ the tensor of electric conductivities. $\mathbf{T}$ is the unknown current vector potential and $\mathbf{T_0}$ is a vector potential which replaces the source field. $\mathbf{W_e}$ and W_n are the edge and nodal test functions. Ω and $\Omega_\mathbf{C}$ are the whole and the conducting domains, respectively. $\mathbf{T}$ satisfies the boundary condition $\mathbf{T}\wedge\mathbf{n}=\mathbf{0}$ on the interface between Ω and Ω_C.

In order to take into account the nonlinearity of magnetic materials, an iterative calculation using the Newton–Raphson method is adopted. Different algorithms to obtain optimal relaxation factor are introduced in our model to get faster and stable convergence [6].

B. Thermal Model

The thermal problem is defined by heat transfer equation [7]

$$\rho C_p\cdot\frac{\partial T}{\partial t}+\mathrm{div}\,(-[\lambda]\cdot\mathbf{grad}T)=P \quad (3)$$

where T, ρ, Cp, $[\lambda]$, P are the temperature, the specific mass, the specific heat, the tensor of thermal conductivity, and the electromagnetic induced volumic power density, respectively.

In the modulated excitation, the specimen is submitted to a sinusoidal modulated power. The time variation term becomes $(\partial/\partial t)=j\omega_{th}$. Where ω_{th} is the modulating pulsation of the heating source. Equation (3) becomes

$$j\rho C_p\omega_{th}\cdot T+\mathrm{div}\,(-[\lambda]\cdot\mathbf{grad}T)=P. \quad (4)$$

As the temperature variation interval is relatively small, the parameters of electromagnetic and thermal problems are set for this range of temperature.

C. Shell Elements Discretization

In thin regions, prismatic elements are introduced. In the discrete formulation of the problem, the volume integrals are replaced by surface integrals using shell elements. The scalar and vector fields are approximated by nodal and edge elements which are developed specifically for thin regions (Fig. 2). Eqs. (1) and (2) are solved with a shell element representation of the thin region.

The nodal and the edge shell elements are used to interpolate Φ and $\mathbf{T}$, respectively. Denoting by W_t^0 and $\mathbf{W_t^1}$ the triangular nodal and edge element spaces, (1) and (2) are transformed to [3]

$$\int_{\Omega_{\mathrm{shell}}}\mathbf{Curl}\,\mathbf{W_{e_i}}[\sigma_{\mathrm{shell}}]^{-1}\mathbf{Curl}\,\mathbf{T}\cdot d\Omega$$
$$=\int_{S_{\mathrm{shell}}}\frac{1}{\delta}[\sigma_{\mathrm{shell}}]^{-1}\left([\boldsymbol{w}^{\mathbf{1}}_{\boldsymbol{tk}^+}-\boldsymbol{w}^{\mathbf{1}}_{\boldsymbol{tk}^-}]-\delta\mathbf{grad_s}w^0_{tn}\right)$$
$$\cdot\left([\mathbf{T_{tk^+}}-\mathbf{T_{tk^-}}]-\delta\mathbf{grad_s}\mathbf{T_{n^\pm}}\right)$$
$$+\int_{S_{\mathrm{shell}}}\delta[\sigma_{\mathrm{shell}}]^{-1}\int_{-\frac{1}{2}}^{\frac{1}{2}}\mathbf{Curl}\left(\boldsymbol{w}^{\mathbf{1}}_{\boldsymbol{tk}^+}\cdot\beta^+-\boldsymbol{w}^{\mathbf{1}}_{\mathbf{tk}^-}\cdot\beta^-\right)$$
$$\cdot\mathbf{Curl}(\mathbf{T_{tk^+}}\cdot\beta^+-\mathbf{T_{tk^+}}\cdot\beta^-) \quad (5)$$
$$\int_{\Omega_{\mathrm{shell}}}\mu_{\mathrm{shell}}\left(\mathbf{w_{e_i}}+\mathbf{grad}w_{n_i}\right)\cdot\left(\mathbf{T}+\mathbf{grad}\Phi\right)\cdot d\Omega$$
$$=\int_{S_{\mathrm{shell}}}\left[\frac{\mu_{\mathrm{shell}}}{\delta}\right]\left(\delta\cdot w^0_{tn^\pm}+\left[w_{tn^+}-w^0_{tn^-}\right]\right)$$
$$\cdot\left(\delta\cdot T_{n^\pm}+\left[\Phi_{tn^+}-\Phi_{tn^-}\right]\right)\cdot dS$$
$$+\int_{S_{\mathrm{shell}}}\delta\cdot\mu_{\mathrm{shell}}\int_{-\frac{1}{2}}^{\frac{1}{2}}\left[\left(\mathbf{w^1_{tk^+}}+\mathbf{grad}w^0_{tn^+}\right)\cdot\beta^+\right.$$
$$\left.+\left(\boldsymbol{w}^{\mathbf{1}}_{\mathbf{tk}^-}+\mathbf{grad}w^0_{tn^-}\right)\cdot\beta^-\right]\cdot\left[\left(\mathbf{w^1_{tk^+}}+\mathbf{grad}w^0_{tn^+}\right)\cdot\beta^+\right.$$
$$\left.+\left(\mathbf{w^1_{tk^-}}+\mathbf{grad}w^0_{tn^-}\right)\cdot\beta^-\right]d\xi dS \quad (6)$$

where $\mathbf{w^1_{tk^+}}$ and $\mathbf{w^1_{tk^-}}$ belong to the triangular edge element space $\mathbf{W_t^1}$. w^0_{tn} belongs to the triangular nodal element space W_t^0. Signs $+$, $-$ and $\pm$ indicate that the unknown belongs to surfaces Γ^+, Γ^- or edges normal to both surfaces. $\mathbf{T_{tk}}$ represents the tangential component of electrical vector potential projected on the edge k. $\mathbf{T_n}$ is its normal component to the median surface S_{shell} of the thin region interpolated by the edge $k^\pm$. The index $\mathbf{t}$ indicates that $\mathbf{T_{tk}}$ belongs to $\mathbf{W_t^1}$. Φ is the magnetic scalar potential discretized by the node n. β^+ and β^- are linear interpolation functions along the axis ξ [3]. σ_{shell} and μ_{shell} are, respectively, the magnetic permeability and the electric conductivity of the thin region.

For nonconducting regions such as cracks, (5) is replaced by the boundary condition $\mathbf{T}\wedge\mathbf{n}=\mathbf{0}$. However, for conducting regions such as thin plates, one should used (5) and (6) simultaneously.

D. Model Validation

Numerical model developed above is validated by comparison with experimental data in the case of health inspection of a ferromagnetic piece. Fig. 1 shows the experimental setup of the thermo-inductive technique. The technique was carried out on a piece of steel XC38 whose dimensions are defined in the Fig. 3(a). A surface crack with a depth of 2.5 mm was inserted in the specimen excited by an electromagnetic field at a frequency of 50 Hz.

The problem was solved by the nonlinear magnetodynamic formulation. The defect was modeled by shell elements.

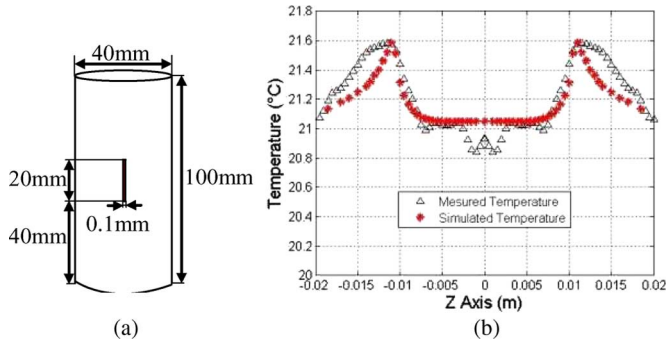

Fig. 3. (a) Modeled piece with crack and (b) simulated and measured temperature distribution along the defect axis after 0.5 s (fr $= 50$ Hz).

The presence of the defect creates the concentration of induced current at the extremities of the default. This concentration generates two hot spots at the defect's extremities. These hot spots are illustrated in Fig. 3(b), where the measured temperature is plotted along the defect axis. On the same figure, the simulation results are compared with experimental data. A relatively good concordance between the two curves is observed. The difference is partly due to the noise in the measurement and variation of the material emissivity.

IV. Applications and Results

Numerical models developed for NDT by thermo-inductive technique have been applied as a support tool for the qualification of the detection process.

A. Contrast Definition

In order to study the defect detection and the influence of various parameters of the system on the characterization of the crack, it is necessary to introduce some discriminating parameters.

1) Thermal Contrast: In the case of pulse stimulation, thermal contrast analysis provides a good indication of defect characteristics. We use the normalized thermal contrast defined by

$$C_i(t) = \frac{T_{\text{def}}(t) - T_{\text{def}}(t_0)}{T_{\text{sdef}}(t) - T_{\text{sdef}}(t_0)} \tag{7}$$

where $C_i(t)$ is the normalized thermal contrast in a point (i) at time t. T_{def}, T_{sdef} are surface temperatures with and without defect in a point (i), and t_0 is the initial time. It can be noticed that the defect detection is better for thermal contrasts different from 1.

2) Phase Contrast: The use of the thermal contrast as a characterization tool is not sufficient because C_i defined in (7) depends on the induced power. To complete it, another parameter called phase contrast is used to quantify the defect. In this approach, the specimen is pulse heated by induction and the phase of the thermal waves is obtained by the Fourier's transform of the temperature evolution for each pixel [8]. Then, the phase contrast is defined by

$$\Delta\Phi_i = \Phi_{i_{\text{def}}} - \Phi_{i_{\text{sdef}}} \tag{8}$$

where $\Delta\Phi_i$ is the phase contrast in a point (i). $\Phi_{i_{\text{def}}}$, $\Phi_{i_{\text{sdef}}}$ are phases with and without defect in the same point. The phase contrast is often used due to its sensitivity to thermal and geometrical properties [8].

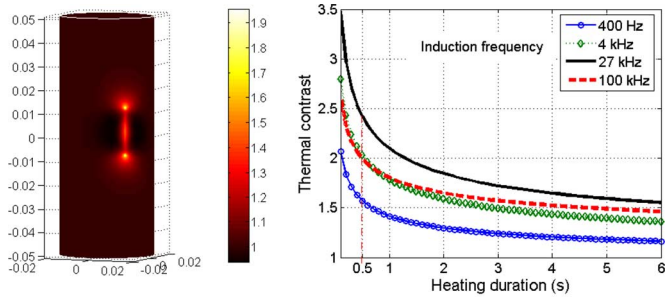

Fig. 4. (a) Image of thermal contrast distribution. (b) Thermal contrast as function of the heating period.

B. Application to Ferromagnetic Materials

The nature of pieces encountered in the industry are various and complex. The study of all kinds of products is out of the scope of this paper. We have applied thus the new method for two main groups of materials in order to demonstrate its relevance. Investigations on some parameters are detailed to show the interest of the developed code.

The first kind is the metallic materials used in automotive industry. To study the feasibility of this technique, the specimen is supposed to be a cylindrical piece of steel XC38 with an open crack of 2.5 mm depth presented in Fig. 3(a) and the inductor chosen is the Helmholtz coil after a study of its performance with a goal function based on the contrasts.

An effective inspection by the thermo-inductive technique depends greatly on the sensitivity of the infrared camera and image processing which increases the defect detection. Indeed, the acquisition and the sampling times depend on the thermal diffusivity of the specimen and the defect depth.

The ferromagnetic pieces have generally a good diffusivity. Thus, the chosen acquisition parameters are relatively low. This leads to a sampling time <0.1 s and acquisition time >5 s.

Heating Time and Electromagnetic Frequency: The numerical model is used to calculate the thermal contrast as a function of the electromagnetic frequency and heating time. Fig. 4(a) shows the cartography of the contrast for a heating time of 0.5 s and a frequency of 100 kHz. The temperature is more contrasted around the crack and the defect is appearing as a line with two hot spots in extremities.

Fig. 4(b) shows the thermal contrast of the hot points calculated versus the heating time. In the case of short heating time, the contrast is larger than 1. With increasing heating duration, the contrast becomes smaller due to the good thermal conductivity of steel. In practice, a heating time about of 0.5 s is a good compromise between the infrared camera detection level, the power of the generator and the contrast.

From this figure, one remarks that the contrast pass by a maximum corresponding to an optimal of the induction frequency which is, in this case, about 27 kHz. Numerical calculations show that the optimal electromagnetic frequency is inversely proportional to cracks depth.

C. Application to Composite Materials

In the aeronautic industry, one of the most observed defects is the delamination in composite plates. This type of defects is difficult to detect with classical techniques of NDT.

In this case, the inspected plates are two carbon fiber reinforced polymer composites with dimensions shown in Fig. 5(b). In one of the plates, a cylindrical delamination is inserted at the

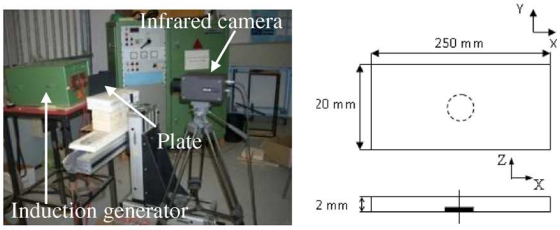

(a) (b)

Fig. 5. (a) Experimental setup. (b) Composite plate with delamination.

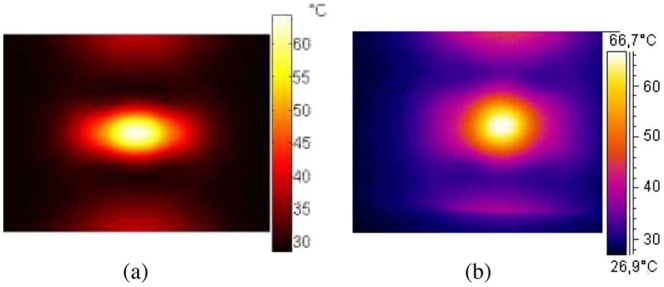

(a) (b)

Fig. 6. (a) Simulated and (b) measured temperature distribution.

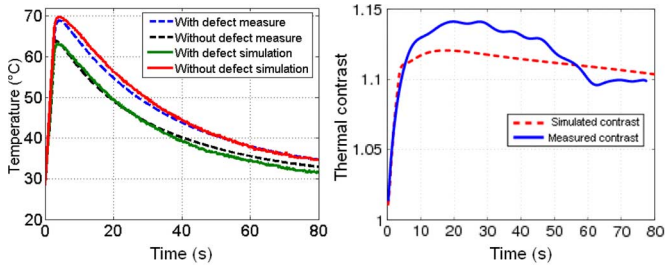

(a) (b)

Fig. 7. Simulated and measured results.

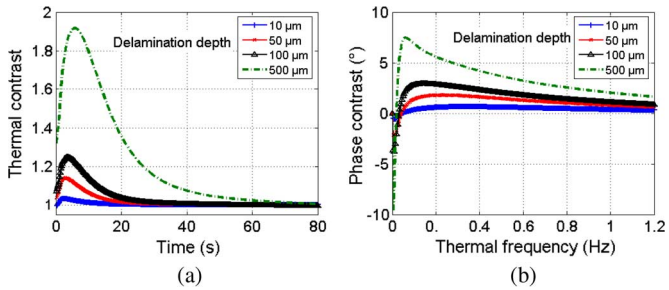

(a) (b)

Fig. 8. (a) Thermal and (b) phase contrasts as function of the delamination depth.

middle height of the plate. This material has anisotropic properties which are taken into account in the model by involving electrical and thermal conductivity tensors. The electrical conductivity is equal to zero in the depth because the layers are separated by an insulating resin.

Fig. 5(a) shows the experimental setup for these materials. An inductor with the form U is chosen after a study of its performance based on the thermal and phase contrasts using the developed code. Due to the low thermal diffusivity of the composite, the acquisition parameters are relatively high leading to a sampling time <0.2 s and acquisition time >60 s.

Fig. 6 presents the measured and the simulated temperature distribution on the lower surface of the plate. The images show a deformation of the hot zone below the inductor which gives information about the delamination form.

To compare the difference between the plate with and without defect, the temporal evolution of the temperature of a point in the centre is shown in Fig. 7(a). The presence of delamination has the effect of increasing surface temperature. For the plate with default, the maximum is 70 °C. While for the plate without defect, the maximum is 63 °C. Similarities between the measured and calculated curves are observed.

In order to deepen this comparison, the thermal contrast is calculated. The comparison between the measured and simulated contrasts shows that there is a small difference which becomes relatively large with increasing observation time. This can be explained by the decrease of the signal compared to the noise [Fig. 7(b)].

Delamination Characterization: Fig. 8 shows the thermal and phase contrasts for a heating period of 1 s. The composite materials have relatively low thermal conductivity in their depth direction. As a consequence, the thermal contrast reaches its maximum value some fraction of seconds after turning off the power source. The results give a good indication of how the composite material responds to thermal excitation. These materials have a low electrical conductivity. Therefore, to obtain an acceptable level of contrast, one should use frequencies higher than 500 kHz. The maximum thermal and phase contrast values increase with the induction frequency.

V. Conclusion

In this paper, the thermo-inductive technique has been studied in order to detect defects. A 3-D numerical model using Whitney's elements is developed as a support tool. Thin regions have been modelled using shell elements. The use of both nodal and edge shell elements permits the interpolation of scalar and vector variables. Experimental data enabled us to validate the finite-elements model developed. Two complementary discrimination parameters were defined to analyze the results which are the thermal and phase contrasts.

Two groups of materials usually encountered in automotive and aeronautic industries have been studied: metallic and composite materials. The numerical model is used to optimize the detection and characterization of defects. It has been shown that the crack detection depends on the heating time, the excitation frequency and the size of defects. For the composites material, the heating time and the electromagnetic frequency are more important that for the metallic pieces. Experimental and simulation results have demonstrated that cracks can be detected and quantified with the thermo-inductive technique.

References

[1] B. Ramdane, D. Trichet, M. Belkadi, and J. Fouladgar, "3D numerical modeling of NDT by thermo-inductive technique," in *Proc 13th IEEE CEFC*, Athens, Greece, May 11–15, 2008, p. 418.

[2] G. Walle and U. Netzelmann, "Thermogrphic crack detection in ferritic steel components using inductive heating," in *Proc. 9th Eur. Conf. Non-Destructive Testing (ECNDT 2006)*, Berlin, Germany, Sep. 2006.

[3] Z. Ren, "Degenerated whitney prism elements—General nodal and edge shell elements for field computation in thin structures," *IEEE Trans. Magn.*, vol. 34, no. 5, pp. 2547–2550, Sep. 1998.

[4] O. Biro and K. Pries, "On the use of the magnetic vector potential in the finite element analysis of 3-D eddy current," *IEEE Trans. Magn.*, vol. 25, no. 4, pp. 3145–3159, Jul. 1989.

[5] A. Bossavit, "A rationale for edge elements in 3-D fields computation," *IEEE Trans. Magn.*, vol. 24, no. 1, pp. 74–79, Jan. 1988.

[6] K. Fujiwara, Y. Okamoto, and A. Kameari, "The Newton-Raphson method accelerated by using a line search—Comparison between energy functional and residual minimization," *IEEE Trans. Magn.*, vol. 41, no. 5, pp. 1724–1727, May 2005.

[7] S. V. Patankar, *Numerical Heat Transfer and Flow Fluid*. Bristol, PA: Hemisphere, 1970.

[8] X. Maldague and S. Marinetti, "Pulse phase infrared thermography," *Eur. Appl. J. Appl. Phys*, vol. 79, no. 5, pp. 2694–2698, 1996.